AD-A136 988 SIMULATION OF EDGE EFFECTS IN ELECTROANALYTICAL EXPERIMENTS BY ORTHOGONAL.. (U) UTAH UNIV SALT LAKE CITY DEPT OF CHEMISTRY J F CASSIDY ET AL. 06 JAN 84 TR-23 1/1

UNCLASSIFIED N00014-83-K-0470 F/G 7/4 NL

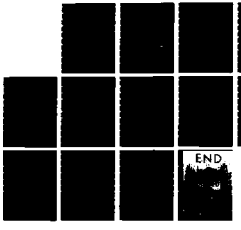

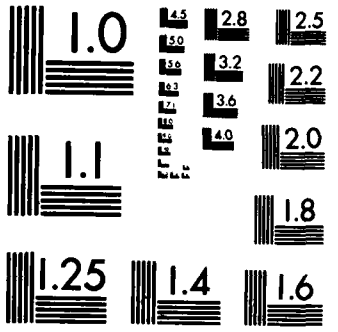

SECURITY CLASSIFICATION OF THIS PAGE (When Data Entered)

REPORT DOCUMENTATION PAGE

READ INSTRUCTIONS BEFORE COMPLETING FORM

1. REPORT NUMBER: 23	2. GOVT ACCESSION NO.
3. RECIPIENT'S CATALOG NUMBER	
4. TITLE (and Subtitle): Simulation of Edge Effects in Electroanalytical Experiments by Orthogonal Collocation. Part 4. Application to Voltammetric Experiments	5. TYPE OF REPORT & PERIOD COVERED: Technical Report # 23
	6. PERFORMING ORG. REPORT NUMBER
7. AUTHOR(s): John F. Cassidy, Stanley Pons, A. Scott Hinman, Bernd Speiser	8. CONTRACT OR GRANT NUMBER(s): N00014-83-K-0470
9. PERFORMING ORGANIZATION NAME AND ADDRESS: University of Utah, Department of Chemistry, Salt Lake City, UT 84112	10. PROGRAM ELEMENT, PROJECT, TASK AREA & WORK UNIT NUMBERS: Task No. NR 359-718
11. CONTROLLING OFFICE NAME AND ADDRESS: Office of Naval Research, Chemistry Program - Chemistry Code 472, Arlington, Virginia 22217	12. REPORT DATE: January 6, 1984
	13. NUMBER OF PAGES
MONITORING AGENCY NAME & ADDRESS (if different from Controlling Office)	15. SECURITY CLASS. (of this report): Unclassified
	15a. DECLASSIFICATION/DOWNGRADING SCHEDULE

AD A136988

DISTRIBUTION STATEMENT (of this Report)

This document has been approved for public release and sale; its distribution unlimited.

DISTRIBUTION STATEMENT (of the abstract entered in Block 20, if different from Report)

DTIC ELECTE JAN 19 1984 A

SUPPLEMENTARY NOTES

18. KEY WORDS (Continue on reverse side if necessary and identify by block number)

Diffusion, Simulation, Collocation, Edge Effects

20. ABSTRACT (Continue on reverse side if necessary and identify by block number)

Orthogonal collocation is used to simulate cyclic voltammograms that are influenced by non-linear diffusion due to edge effects at small disc electrodes.

DTIC FILE COPY

DD FORM 1473 EDITION OF 1 NOV 65 IS OBSOLETE S/N 0102-LF-014-6601

Unclassified

SECURITY CLASSIFICATION OF THIS PAGE (When Data Entered)

84 01 17 125

OFFICE OF NAVAL RESEARCH

Contract N00014-83-K-0470

Task No. NR 359-718

TECHNICAL REPORT NO. 23

Simulation of Edge Effects in Electroanalytical Experiments by Orthogonal Collocation. Part 4. Application to Voltammetric Experiments

By

John F. Cassidy
Stanley Pons*
A. Scott Hinman
Bernd Speiser

Prepared for Publication In

Canadian Journal of Chemistry

University of Utah
Department of Chemistry
Salt Lake City, Utah 84112

January 6, 1984

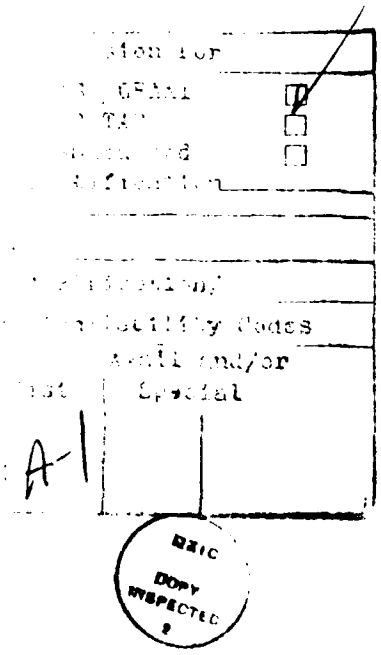

Simulation of Edge Effects in Electroanalytical Experiments by Orthogonal Collocation. Part 4. Application to Voltammetric Experiments

John F. Cassidy, Stanley Pons*
Department of Chemistry
University of Utah
Salt Lake City, UT 84112

A. Scott Hinman
Department of Chemistry
University of Calgary
Calgary, Alberta, Canada

Bernd Speiser
Institut für Organische Chemie
Universität Tübingen, auf der Morgenstelle 18
D-7400 Tubingen, West Germany

*To whom all correspondence should be addressed.

ABSTRACT

Orthogonal collocation is used to simulate cyclic voltammograms that are influenced by non-linear diffusion due to edge effects at small disc electrodes.

Introduction

In this paper, the general theory derived in part 2 of this series is implemented, and the effect of edge diffusion on the cyclic voltammetric response at very small electrodes is examined. The use of very small electrodes for cyclic voltammetric experiments has usually been limited to specialized investigations, for example in neurochemical studies (1,2). There are obvious advantages in using very small electrodes. In theory, the ratio of the faradaic to the double layer charging current increases with decreasing electrode area. Small electrodes are suited for experiments where available volumes of analyte are limited. In general, several effects have been observed in various systems as the electrode size was reduced. Thus increased faradaic peak separation (3), little or no reverse sweep currents (4,5), and a steady state current plateau (6) have been observed. In the case of a small hanging mercury drop electrode, anomalous behavior was observed when the reduced species was soluble in the mercury drop (7,8,9). The resulting ratio of the reverse peak current to the forward peak current was found to be greater than one.

Examination of the so-called "edge-effect" has been carried out for chronoamperometric experiments (10,11). The analysis by various workers has led to a correction term σ to the Cottrell equation

$$i = nFAC^0\left(\frac{D}{\pi t}\right)^{1/2}\left[1 + \sigma\left(\frac{Dt}{r_0^2}\right)^{1/2}\right] \qquad [1]$$

where r_0 is the electrode radius, and σ varies between 1.772 and 2.257 (11, 12). Using implicit finite difference methods, Heinze developed an analogous equation for the cyclic voltammetric response with contribution from edge effects (6):

$$x_{TOTAL} = x_{i,d}(at) + \rho(at)\sqrt{\beta'}/\sqrt{\pi} \qquad [2]$$

with $\beta' = D/ar_0^2$, $a = nFv/RT$, v = sweep rate. $x_{i,d}(at)$ is the planar diffusion current function and the second term is the radial diffusion current function. In this work, we give the results for the voltammetric response in terms of the efficient orthogonal collocation technique (13,14), the results of which, in many cases, are exact.

The term "very small electrodes" (e.g. 3-300 μm radius (5)) is used herein to differentiate them from microelectrodes, diffusion to which is purely hemispherical. The case examined here is that where the amount of hemispherical diffusion to a planar disk electrode is large enough to cause significant departure in the response from semi-infinite linear diffusion theory. Extentions to the two limiting cases will be discussed.

The solution of the non-linear partial differential equations describing this case has been treated in part 2 (15). The general method is the simulation of the concentration profiles in the diffusion layer by approximate trial functions in distance whose time dependent coefficients are selected by weighted residual techniques such that the differential equation is satisfied at chosen fixed (collocation) points in the distance

coordinate. These points are also chosen purposely as the roots of orthogonal polynomials, combinations of which best approximate the expected profiles and the boundary conditions. The model used herein accounts for planar and lateral diffusion. As has been pointed out (16), it is a simple matter to add homogeneous reactions to the overall scheme once the basic model is developed. The reliability and accuracy of the model have been verified in part 3 (17) of the series, where the chronoamperometric response was simulated.

Theory

The full description of the theory is given in part 2, (15) and is briefly summarized here. The mechanism considered was an EC type:

$$A \underset{+ne^-}{\overset{-ne^-}{\rightleftharpoons}} B \qquad E^\circ \qquad [3]$$

$$B \rightarrow C \qquad k \qquad [4]$$

In this paper, we will not consider the effects of [4], i.e. we let $\alpha = 0$ and the electrode geometry is a planar disk electrode of radius r_0, flush mounted in an insulating cylinder. The diffusion coefficients D_i for all of the species are assumed to be equal, even though the treatment is only slightly different if different D_i are used (13). For this system, the current density will not be homogeneous across the electrode surface, but will be greater near the edges due to additional diffusion to the edge from the region over the insulator. Dimensionless diffusion equations describing the model are

$$\frac{\partial c^*_{A_1}}{\partial T'} = \beta \frac{\partial^2 c^*_{A_1}}{\partial X^2} + \frac{\beta'}{R} \frac{\partial c^*_{A_1}}{\partial R} + \beta' \frac{\partial^2 c^*_{A_1}}{\partial R^2} \qquad [5]$$

$$\frac{\partial c^*_{B_1}}{\partial T'} = \beta \frac{\partial^2 c^*_{B_1}}{\partial X^2} + \frac{\beta'}{R} \frac{\partial c^*_{B_1}}{\partial R} + \beta' \frac{\partial^2 c^*_{B_1}}{\partial R^2} - \alpha c^*_{B_1} \qquad [6]$$

$$\frac{\partial c^*_{C_1}}{\partial T'} = \beta \frac{\partial^2 c^*_{C_1}}{\partial X^2} + \frac{\beta'}{R} \frac{\partial c^*_{C_1}}{\partial R} + \beta' \frac{\partial^2 c^*_{C_1}}{\partial R^2} + \alpha c^*_{C_1} \qquad [7]$$

where the subscript 1 denotes the concentrations above the electrode surface. A similar set of equations exists for the area above the insulator.

The terms in the equations are:

$$\beta = \frac{D}{aL^2}, \quad \beta' = \frac{D}{ar_0^2}, \quad \beta'' = \frac{D}{a(M-r_0)^2}, \quad \alpha = \frac{k}{a}, \quad c^* = \frac{c}{c_A^0} \qquad [8]$$

where $a = nFv/RT$. L represents that distance out in solution above the electrode where no diffusion occurs and M the radial distance out into solution from the center of the electrode where no diffusion occurs. These terms need to be included to normalize the equations later to a (0, 1) distance coordinate so that Legendre polynomials might be used to represent the concentration solutions (15, 17). r_0 is the radius of the electrode and the other terms have their usual significance.

The constant β' is a quantity given by experimental parameters. For simplicity herein we let $\beta = \beta''$. This is a sensible approximation since both L and M are $>> r_0$. The choice of β may be optimized by various procedures already described (18,19). β in essence defines a "window" on the diffusion phenomena. If β is too small, the diffusion layer will be small compared to the collocation point span, and it will be poorly simulated or missed entirely. If, on the other hand, β is chosen too large, then the diffusion effects may be present at L or M

and the boundary conditions will be violated. This is the intuitive reason for optimization of β values. The procedure for optimization depends on the integration method used for solution of the set of differential equations. Each such integration method will have a corresponding set of stability and accuracy criteria which vary significantly from method to method. In the Hammings predictor-corrector method used herein, the stability criterion (20) takes the form

$$h < \frac{0.65}{|f_y|} \qquad [9]$$

where h is the independent variable stepwidth chosen for the integration, and f_y is the Jacobian or derivative of the differential equation f(x,y) with respect to the independent variable at each point of interest. Thus, accuracy and curve shape relax as h is made very small, whereas unstable oscillation will occur if h is too large.

The corresponding first order differential equations for the problem (Part 2 (15)) are:

$$\left.\frac{dc^{*}_{A1}}{dT'}\right|_{X_i,R_k} = \beta \left\{ - \frac{B_{i,1}\theta_{A/B}S_{\lambda}(T')}{A_{1,1}[1 + \theta_{A/B}S_{\lambda}(T')]} \left[A_{1,N_x+2} + \sum_{j=2}^{N_x+1} A_{1,j}[c^{*}_{A1}(X_j,R_k,T') \right.\right.$$

$$\left.\left. + c^{*}_{B1}(X_j,R_k,T')] \right] + B_{i,N_x+2} + \sum_{j=2}^{N_x+1} B_{i,j}c^{*}_{A1}(X_j,R_k,T') \right\}$$

$$+ \frac{\beta'}{G_1} \left\{ \sqrt{\frac{\beta''}{\beta'}}\, I_{1,k}C'_{N_R+2,1} + \sum_{i=2}^{N_R+1} [J_{1,k}(\sqrt{\frac{\beta''}{\beta'}}\, C'_{i,1} - C_{N_R+2,N_R+2}) - I_{1,k}C_{1,} \right.$$

$$\left. + I_{1,k}C_{1,N_R+2}]\, c^{*}_{A1}(X_i,R_1,T') + \sum_{i=2}^{N_R'+1} \sqrt{\frac{\beta''}{\beta'}}\, I_{1,k}C'_{i,1}\, c^{*}_{A2}(X_i,R'_1,T') \right\}$$

[10]

$$\left.\frac{dc^{*}_{B1}}{dT'}\right|_{X_i,R_k} = \beta \left\{ - \frac{B_{i,1}}{A_{1,1}[1+\theta_{A/B}S_{\lambda}(T')]} \right.$$

$$\left[A_{1,N_x+2} + \sum_{j=2}^{N_x+1} A_{1,j}[c^{*}_{A1}(X_j,R_k,T') + c^{*}_{B1}(X_j,R_k,T')] \right]$$

$$\left. + \sum_{j=2}^{N_x+1} B_{i,j} c^{*}_{B1}(X_j,R_k,T') \right\} + \frac{\beta'}{G_1} \left\{ \sum_{l=2}^{N_R+1} [J_{l,k}(\sqrt{\frac{\beta''}{\beta'}}\, C'_{1,1} - C_{N_R+2,N_R+2}) \right.$$

$$- I_{1,k} C_{1,N_R+2}$$

$$\left. + I_{1,k} C_{1,N_R+2}] c^{*}_{B1}(X_i,R_l,T') + \sum_{l=2}^{N_R+1} \sqrt{\frac{\beta''}{\beta'}}\; I_{1,k} C'_{l,1} c^{*}_{B2}(X_i,R_l,T') \right\} - \alpha\, c^{*}_{B1}$$

[11]

$$\left.\frac{dc^{*}_{A2}}{dT'}\right|_{X_i,R'_k} = \frac{\beta}{A_{1,1}}\left\{K_{i,N_x+2} + \sum_{j=2}^{N_x+1} K_{i,j}c^{*}_{A2}(X_j,R'_k,T')\right\}$$

$$+ \frac{\beta''}{G_1}\left\{L'_{N_{R'}+2,k} + \sum_{l=2}^{N_R+1} F_{1',k}H_l c^{*}_{A1}(X_i,R_l,T') + \sum_{l=2}^{N_{R'}+1} L'_{l,k}c^{*}_{A2}(X_i,R'_l,T')\right\}$$

[12]

$$\left.\frac{dc^{*}_{B2}}{dT'}\right|_{X_i,R'_k} = \frac{\beta}{A_{1,1}}\left\{\sum_{j=2}^{N_x+1} K_{i,j}c^{*}_{B2}(X_j,R'_k,T')\right.$$

$$\left. + \frac{\beta''}{G_1}\sum_{l=2}^{N_R+1} F_{1',k}H_l c^{*}_{B1}(X_i,R_l,T') + \sum_{l=2}^{N_{R'}+1} L'_{l,k}c^{*}_{B2}(X_i,R'_l,T')\right\} - \alpha c^{*}_{B2}$$

[13]

The A_i, B_i, C_i, F_i, G_i, H_i, J_i, K_i, and $\;_i$ are discretization matrix elements which have been defined previously (15, 17).

The Jacobians of each of these expressions are

$$f_1 = \frac{\partial}{\partial c^*_{A_1}}\left(\frac{dc^*_{A_1}}{dT'}\right); \quad f_2 = \frac{\partial}{\partial c^*_{B_1}}\left(\frac{dc^*_{B_1}}{dT'}\right);$$

$$f_3 = \frac{\partial}{\partial c^*_{A_2}}\left(\frac{dc^*_{A_2}}{dT'}\right); \quad f_4 = \frac{\partial}{\partial c^*_{B_2}}\left(\frac{dc^*_{B_2}}{dT'}\right) \qquad [14]$$

We then specify the two limiting cases at $S_\lambda(T') = 1$ (at the beginning of the experiment), and $S_\lambda(T') = 0$ (at the end of the experiment). Thus there are six total conditions to be treated by the iteration procedure described previously (14,19) so that the optimum value of β for a given steplength is obtained.

Results and Discussion

The program was first tested under conditions of semiinfinite linear diffusion and the resulting values of the current function $\chi(at)$ compared well with those of Nicholson and Shain (21) ($\chi(at) = 0.44627$ at $\beta' = 10^{-10}$, $\beta = 0.05$, and $\Delta E_p = 0.057$ V). Various combinations of α and switching potentials were used to vary the parameter log $(k\tau)$ where τ is the time between E° and E_λ governed by the scan rate, and k is the homogeneous rate constant for the follow-up reaction. The results are shown in Figure 1. This verifies the consistancy of the model at low values of β'. For any value of β' chosen, the corresponding value of β is optimized by iteration and it makes little difference what original value of β is input since rapid convergence to the optimum value is manifest.

The general shape of the voltammograms may be predicted with reference to the factor β. When β is small, the corresponding value of L is large and the radius is small with respect to L. Thus the factor

$$\beta' = \left[\frac{D}{\left(\frac{nFv}{RT}\right) r_0^2}\right] \qquad [15]$$

contributes more to the current function and we reach a steady state at faster times.

If, on the other hand, β is large then L is small relative to r_0 so that the spherical diffusion effects are less and a more classical voltammogram is expected. The ratio $\sqrt{\beta/\beta'}$ equals r_0/L

and the effect of this factor on the shape and magnitude of the current function are shown in Figure 2. Curves (a) and (b) are calculated for the case when β is not optimized. Thus they have the apperance of voltammograms from microelectrodes. However r_0 for curve (a) is 113 μm whereas for curve (c) r_0 is 9 μm (D_0 = 10^{-6} cm^2/sec, v = 1 V/s). The effect of optimizing the parameter β for curve (c) is the scaling down of the surrounding dimensions to accommodate the small radius. Thus the voltammogram has a classical shape. This does not occur physically and for very small radii a voltammogram of the form (a) is observed which can be easily simulated with the appropriate value of β.

Figure 3 shows the effect of β' on the current function. At small values of β' the classical value of 0.4463 is obtained. At large values there is an asymptotic approach to hemispherical diffusion values.

Anomalous forward/reverse peak current ratios have been observed at small hanging mercury drop electrodes. Beyerlein and Nicholson (7) have pointed out that these are caused by both sphericity and amalgam formation and have demonstrated the dependance of the magnitude on $\sqrt{\beta'}$. Guminski and Galus (8) developed an experimental equation for the resulting ratio

$$\frac{i_{pr}}{i_{pf}} = -\left[1 + 3.2\sqrt{\frac{D_{red}(E_{pc}-E_{\lambda})}{vr_o^2}}\right] \qquad [16]$$

The spherical correction obviously becomes less at large drop sizes and/or high sweep rates.

Galus has presented a spherical correction equation for

small planar disks (22)

$$\frac{i_{pf}}{i_{pr}} = \{1 + Q' \sqrt{\beta'}\} \qquad [17]$$

Q' was estimated as 0.92 by oxidizing ferrocyanide at a graphite paste planar disk electrode (r_0 = 81 μm). At low scan rates, however, there was no reverse current observable.

In the model presented herein for small planar disks there is no evidence for departure from the current ratio of unity due to edge effects. In practice, it is probably true that the small but not negligible charging current contributes to the observed results.

Beyerlein and Nicholson (7) have presented an equation for the current function at a hanging mercury drop electrode in terms of a linear combination of planar and spherical components:

$$\chi(at) = \chi(0)_{i,d} + A\beta' + B\sqrt{\beta'} \qquad [18]$$

If the equation is rearranged, it is seen that a plot of

$$\frac{\chi(at) - \chi(0)_{i,d}}{\sqrt{\beta'}} \qquad [19]$$

vs $\sqrt{\beta'}$ should yield a straight line for a system having spherical diffusion contribution. It is seen in Figure 4 that such a plot constructed with the present model leads to an intercept, when extrapolation is made from large β' values (small r_0), which is equivalent to the value obtained by Beyerlein and Nicholson for a

peak current function value. This indicates the model is correctly providing currents consistent with pure hemispherical diffusion at large values of β'.

Recently an expression for the current in the following form was proposed (23):

$$i(t) = i_{i,d}(t) + \frac{i_1(t)}{r_0} + \frac{i_2(t)}{r_0^2}t + ... \qquad [20]$$

the second term being found analytically in the case of the potential scan. The calculated value for B from the first two terms compares well with that of Beyerlein and Nicholson (7).

It is observed that, as different values of the integration stepwidth h were chosen, the product of the optimized value of β and h is a constant. The reason for this becomes clear as the following points are considered. We assume that the diffusion layer thickness δ has grown to some value

$$\delta^2 = \pi D \Delta t \qquad [21]$$

after some time interval Δt. It is noted again that L^2 is related to δ^2 through the definition of β. Thus any change in Δt by a factor Q' implies a necessary 1/Q' factor change in β to preserve the relative values of δ and L. This, of course, is true only at the optimized β value for a given h. Thus if an optimized β,h pair is known, it is unnecessary to re-optimize β if a new value of h is used, or conversely, it is unnecessary to calculate a new h by trial and error if it is desired to use a

specific value of β.

The model also provides a convenient method for obtaining diffusion coeficients or n values. Such a working curve is presented in Figure 5. The predicted change in ΔE_p is plotted vs log β'. The diffusion coefficient is then given by

$$D = \frac{\beta' n F v r_0^2}{RT} \qquad [22]$$

where β' is obtained at the observed value of ΔE_p on the working curve.

Figures 6 and 7 demonstrate the effect on the current function and peak separation of changing the value of the parameter β for a given value of β'. The optimized values of β are indicated.

Acknowledgements

The authors thank the Office of Naval Research, Washington, D.C., for support of part of this work.

References

1. A.G. Ewing, M.A. Dayton, R.M. Wightman, Anal. Chem. 53 (1981) 1842.
2. R.M. Wightman, Anal. Chem. 53 (1981) 1125A.
3. R. Lines, V.D. Parker, Acta Chem. Scand. B31 (1977) 369.
4. M.A. Dayton, J.C. Brown, K.J. Stutts, R.M. Wightman, Anal. Chem. 52 (1980) 946.
5. Z. Galus, J.O. Schenk, R.N. Adams, J. Electroanal. Chem. 135 (1982) 1.
6. J. Heinze, Ber. Bunsenges. Phys. Chem. 85 (1981) 1096.
7. F.H. Beyerlein, R.S. Nicholson, Anal. Chem. 44 (1972) 1647.
8. C. Guminski, Z. Galus, Rocz. Chem. 43 (1969) 2147.
9. J.E. Spell, R.H. Philp, Jr., Anal. Chem. 51 (1979) 2287.
10. K.B. Oldham, J. Electroanal. Chem. 122 (1981) 1.
11. K. Aoki, J. Osteryoung, J. Electroanal. Chem. 122 (1981) 19.
12. J. Heinze, J. Electroanal. Chem. 124 (1981) 73.
13. S. Pons, Can. J. Chem. 59 (1981) 1538.
14. B. Speiser, S. Pons, A. Rieker, Electrochimica Acta 27 (1982) 1171.
15. B. Speiser, S. Pons, Can. J. Chem. 60 (1982), 2463.
16. B. Speiser, A. Rieker, J. Electroanal. Chem. 102 (1979) 1.
17. B. Speiser, S. Pons, Can. J. Chem. 61 (1983), 156.
18. L.F. Whiting, P.W. Carr, J. Electroanal. Chem. 81 (1977) 1.
19. B. Speiser, J. Electroanal. Chem. 110 (1980) 69.

20. A. Ralston in A.H. Ralston and H.S. Wilf, "Mathematical Methods for Digital Computers", Wiley, New York-London, 1960, p. 95.

21. R.S. Nicholson, I. Shain, Anal. Chem. 36 (1964) 706.

22. Z. Galus, J.O. Schenk, R.N. Adams, J. Electroanal. Chem. 135 (1982) 1.

23. J. Goodisman, J. Electroanal. Chem. 144 (1983), 33.

Figure Legends

Figure 1. Ratio of peak currents as a function of log(k_T) curve from Nicholson and Shain points calculated at $\beta' = 10^{-6}$ and β optimized at 0.01089.

Figure 2. Curve (a), $\beta = 2.5 \times 10^{-6}$; $\beta' = 2 \times 10^{-4}$, $r_0/L = 0.112$. Curve (b), $\beta = 10^{-5}$, $\beta' = 2 \times 10^{-4}$, $r_0/L = 0.223$. Curve (c), $\beta = 0.0081$, $\beta' = 0.03162$, $r_0/L = 0.506$. (β optimized).

Figure 3. Effect of β' on the magnitude of peak current function (β optimized).

Figure 4. Plot of $\pi(\chi - \chi_{id})/\sqrt{\beta'}$ against $\sqrt{\beta'}$ showing the transition between the two limiting cases of semi-infinite linear diffusion and hemispherical diffusion.

Figure 5. Working curve for determining D from ΔE where $\beta' = D/ar_0^2$ ($a = nFv/RT$) (β optimized; T = 25°C).

Figure 6. The effect of changing the parameter β on the current function.

Figure 7. The effect of changing β on the peak separation.

Figure 1

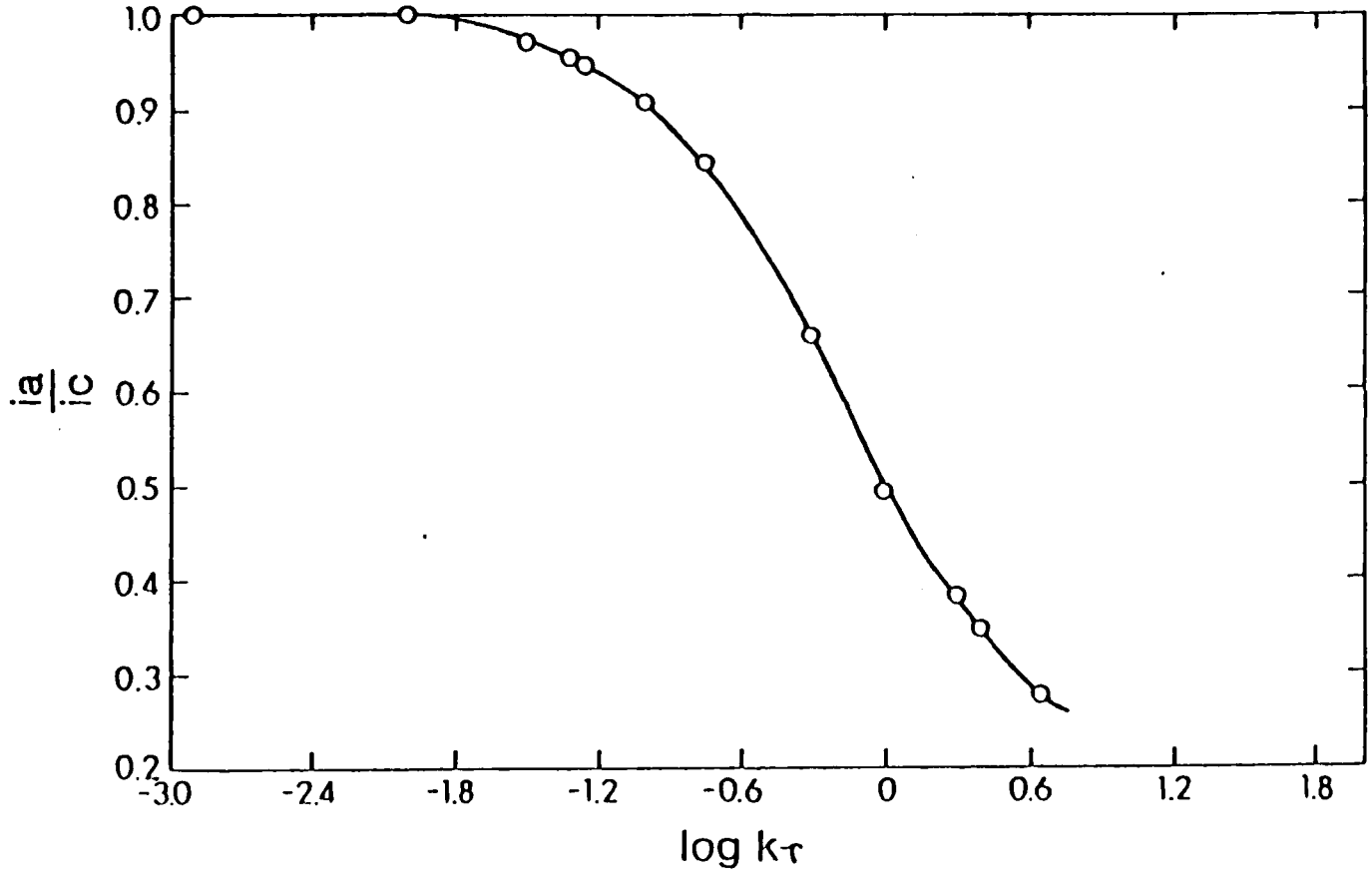

Figure 2

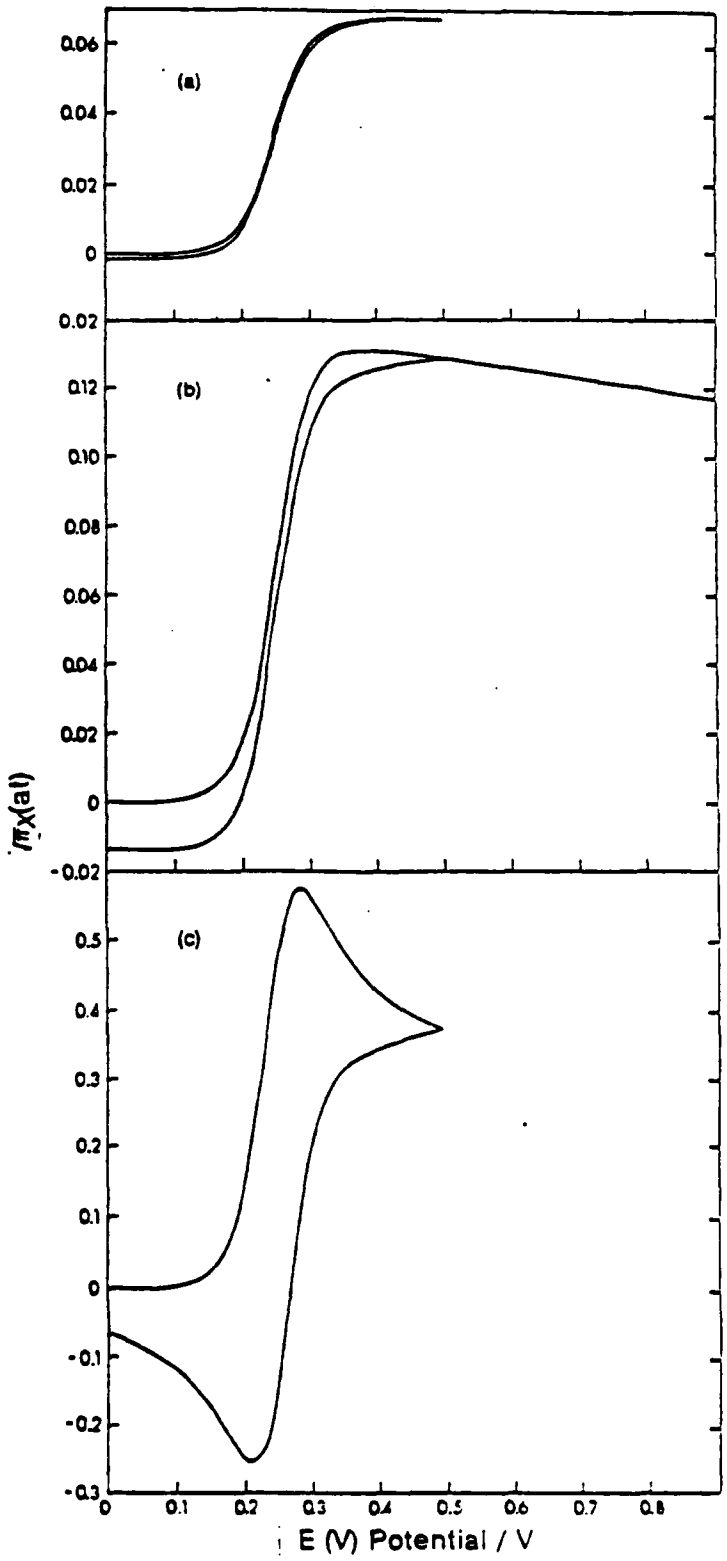
(a)
(b)
(c)
0.06
0.04
0.02
0
-0.02
0.12
0.10
0.08
0.06
0.04
0.02
0
-0.02
0.5
0.4
0.3
0.2
0.1
0
-0.1
-0.2
-0.3
0
0.1
0.2
0.3
0.4
0.5
0.6
0.7
0.8
E (V) Potential / V

Figure 3

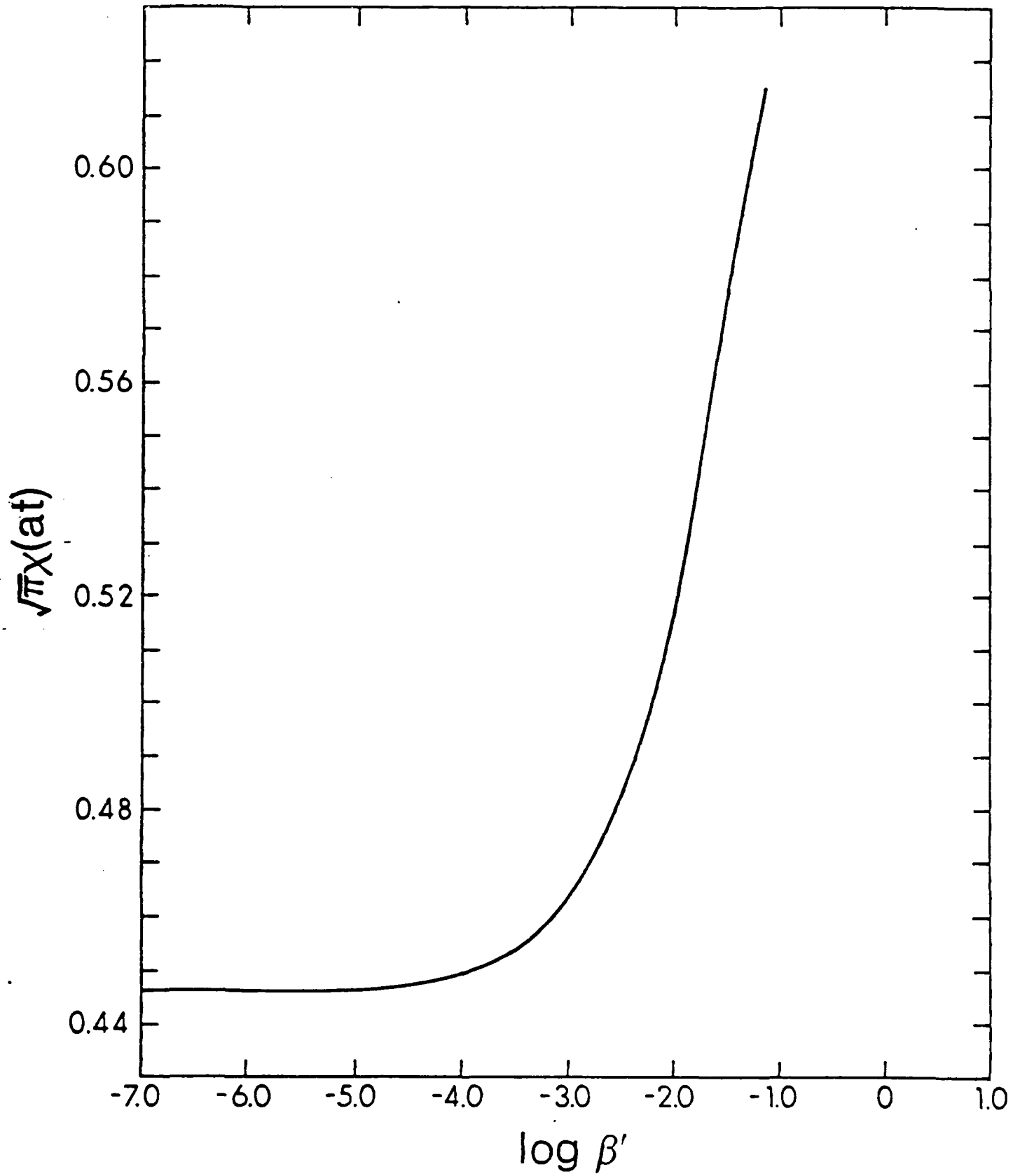
0.60
0.56
0.52
0.48
0.44
$\sqrt{\pi}\chi(at)$
-7.0
-6.0
-5.0
-4.0
-3.0
-2.0
-1.0
0
1.0
log β'

Figure 4

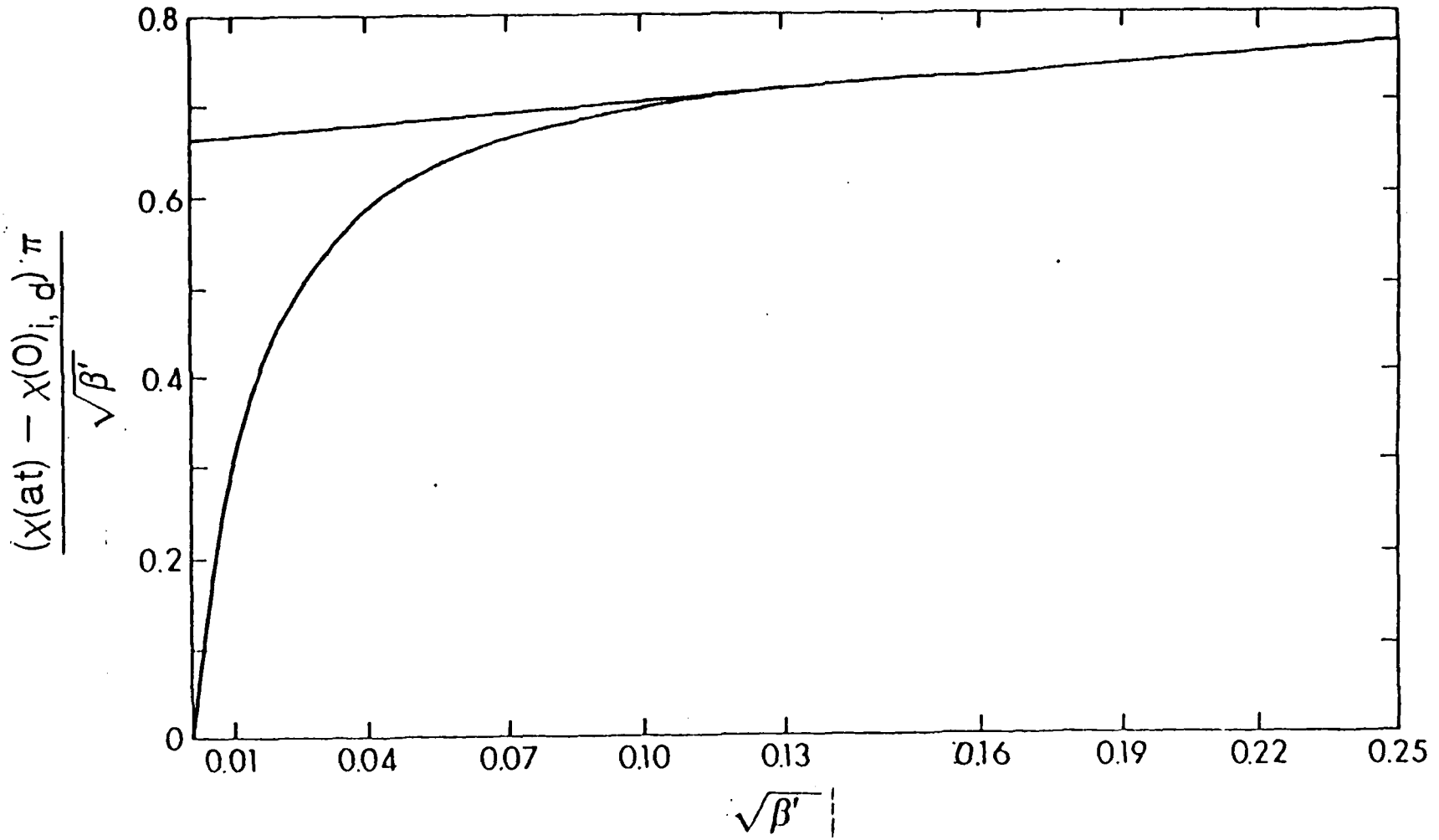
0.8
0.6
0.4
0.2
0
0.01
0.04
0.07
0.10
0.13
0.16
0.19
0.22
0.25
$\frac{(\chi(at) - \chi(0)_{i,d})\cdot\pi}{\sqrt{\beta'}}$
$\sqrt{\beta'}$

Figure 5

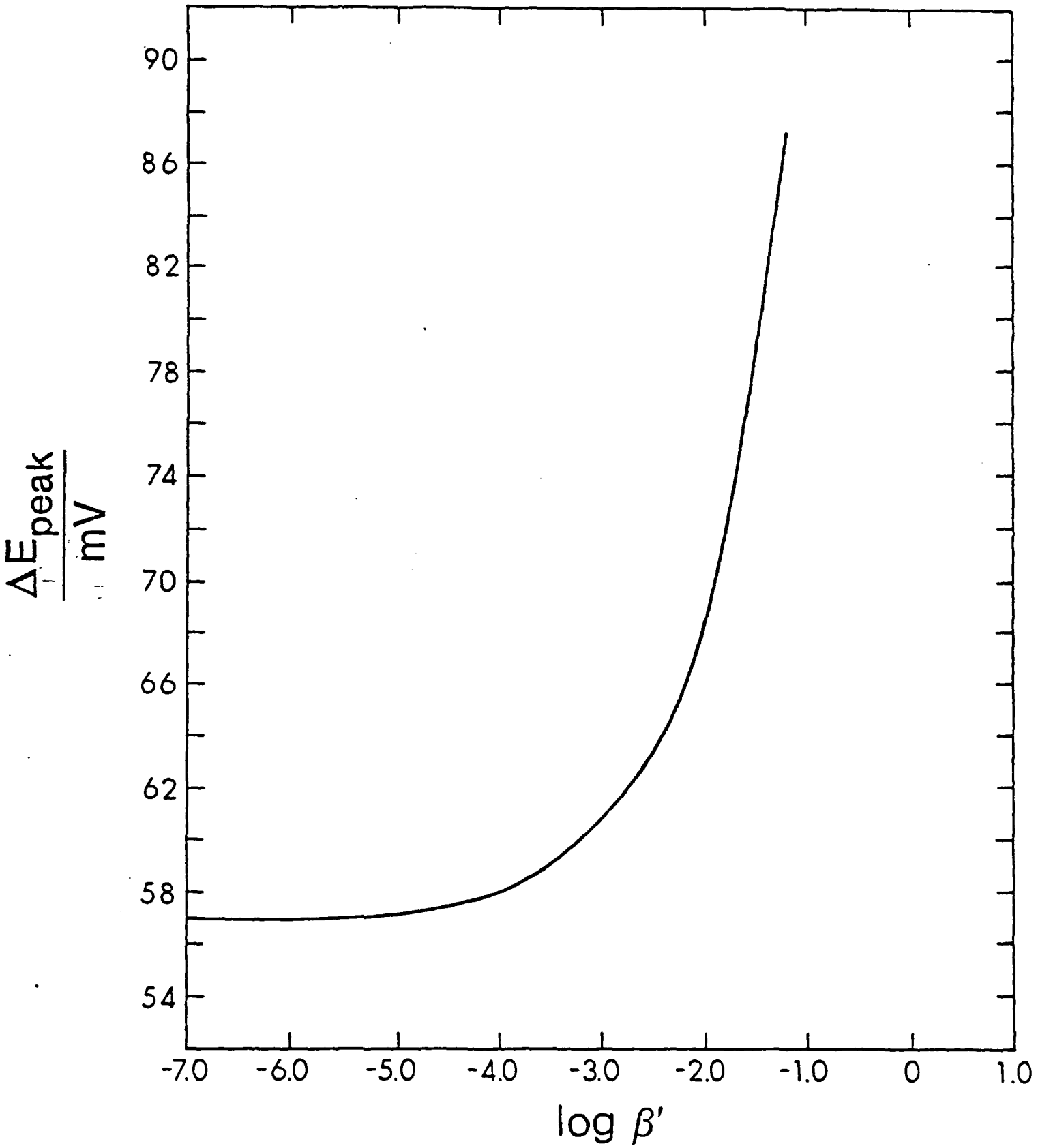
90
86
82
78
74
70
66
62
58
54
$\frac{\Delta E_{peak}}{mV}$
-7.0
-6.0
-5.0
-4.0
-3.0
-2.0
-1.0
0
1.0
log β'

Figure 6

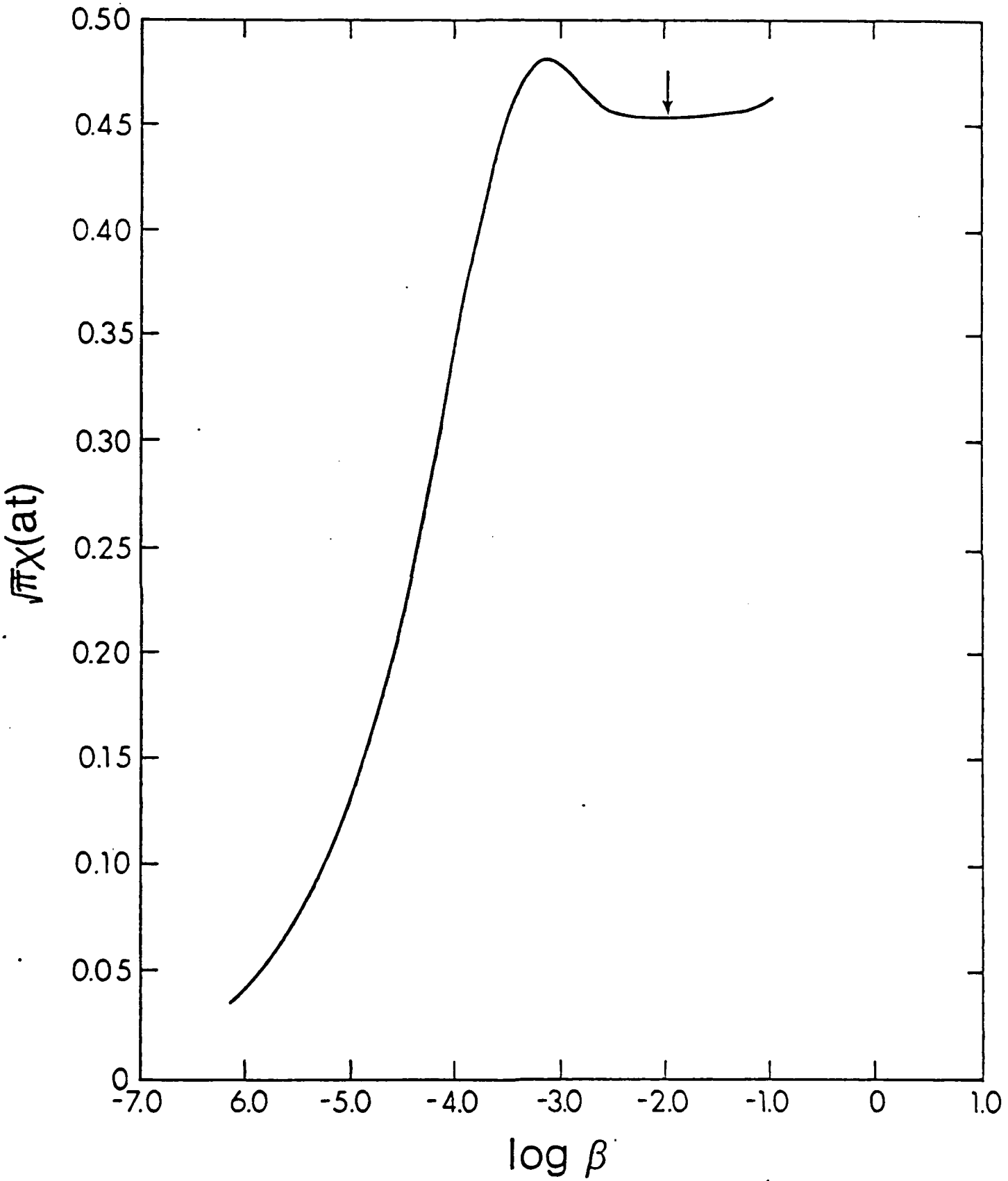
0.50
0.45
0.40
0.35
0.30
0.25
0.20
0.15
0.10
0.05
0
√πχ(at)
-7.0
6.0
-5.0
-4.0
-3.0
-2.0
-1.0
0
1.0
log β

Figure 7

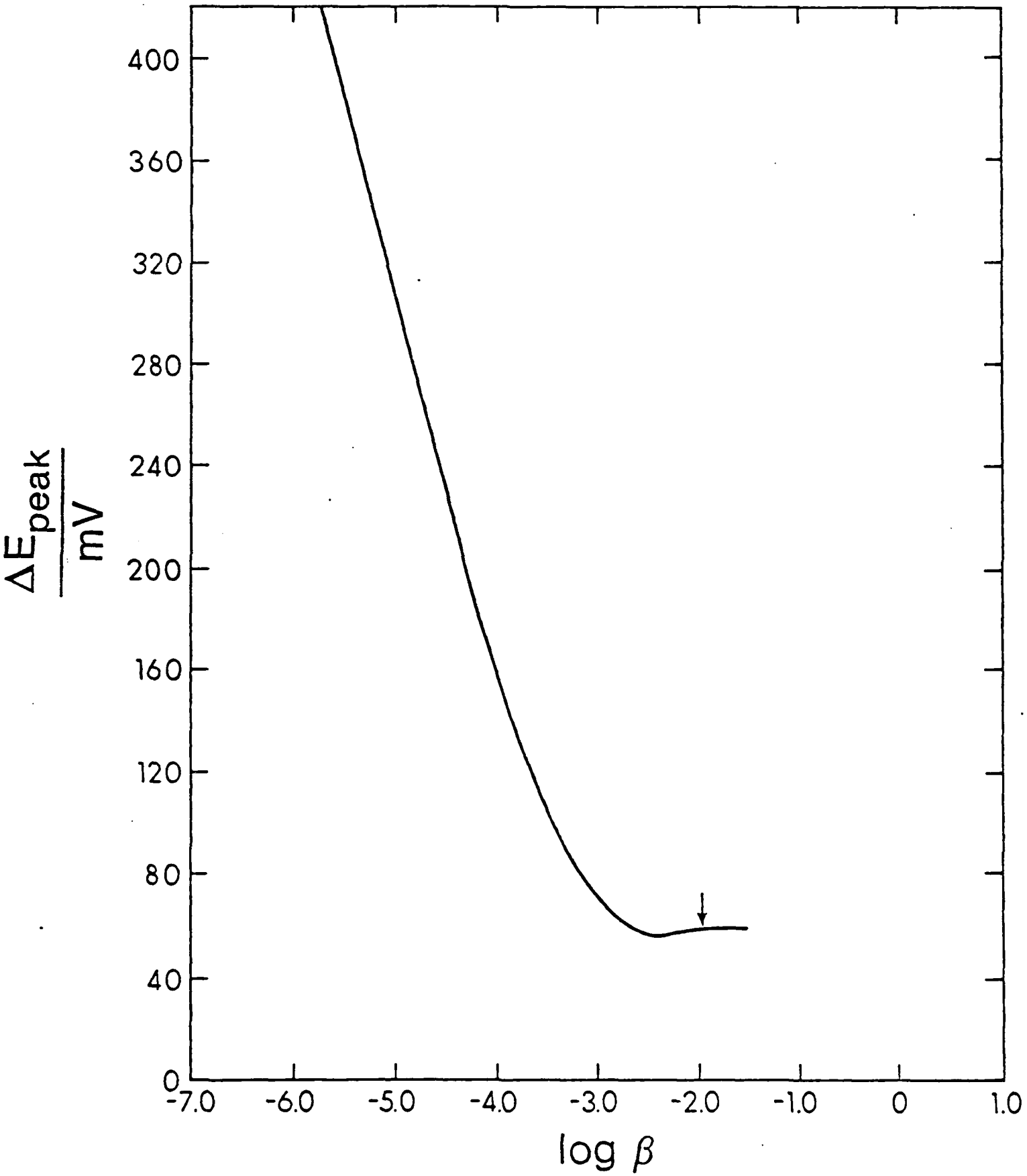
400
360
320
280
240
200
160
120
80
40
0
$\frac{\Delta E_{peak}}{mV}$
-7.0
-6.0
-5.0
-4.0
-3.0
-2.0
-1.0
0
1.0
log β

END

FILMED

2-84

DTIC